Exploring the crystal landscape of 3-methyl-2-phenylbutyramide: crystallization of metastable racemic forms from the stable conglomerate

Udaya Bhaskara Rao Khandavilli, Declan Gavin, Anita R. Maguire, Michael Nolan, and Simon E. Lawrence

Cryst. Growth Des., **Just Accepted Manuscript** • DOI: 10.1021/acs.cgd.8b00348 • Publication Date (Web): 24 Apr 2018

Exploring the crystal landscape of 3-methyl-2-phenylbutyramide: crystallization of metastable racemic forms from the stable conglomerate

U. B. Rao Khandavilli,[†] Declan P. Gavin,[‡] Anita R. Maguire,[‡] Michael Nolan[§] and Simon E. Lawrence[*,†]*

[†] *School of Chemistry, Analytical and Biological Chemistry Research Facility, Synthesis and Solid State Pharmaceutical Centre, University College Cork, Ireland. E-mail: simon.lawrence@ucc.ie*

[‡] *School of Chemistry and School of Pharmacy, Analytical and Biological Chemistry Research Facility, Synthesis and Solid State Pharmaceutical Centre, University College Cork, Cork, Ireland.*

§ *Tyndall National Institute, University College Cork, Lee Maltings, Prospect Row, Cork, Ireland*

RECEIVED DATE (to be automatically inserted after your manuscript is accepted if required according to the journal that you are submitting your paper to)

KEYWORDS: Conglomerate, Polymorphism, DFT calculations and crystallization.

Abstract:

In the solid state (±)-3-methyl-2-phenylbutyramide **1** spontaneously resolves into a conglomerate (Form I) that crystallizes in a racemic form (Form II) upon melting followed by vapor crystallization, a rarely reported phenomenon. An additional racemic polymorph, Form III, has been characterized, and the thermodynamic relationship between the three forms established by a variety of computational and experimental methods including grinding, slurry crystallization and seeding techniques. Both racemic Forms II and III are metastable and readily convert to the more stable conglomerate, Form I. Density Functional Theory calculations of the different polymorphs of **1** show that the enantiomers of **1** (*R* & *S*) are more stable than both racemic forms.

Introduction:

The racemic and enantiopure forms of a pharmaceutical compound often display distinct physiological and pharmacological properties in living organisms.[1-3] Many chiral pharmaceutical compounds in the market were historically developed as racemates.[4] Specific guidelines for the

marketing of the bio-active enantiomer of an active pharmaceutical ingredient (API) have been provided by the FDA since 1992, to ensure safety.[5-6] These directives stipulate that each isomer and racemic form of an API should be studied separately to understand their pharmacological activity and metabolic pathways. Therefore, obtaining enantiopure compounds has received tremendous attention from both academic and industrial researchers over the last few decades.[7] This has provided a strong stimulus for the development of methodologies for the asymmetric synthesis of organic compounds.[8] From the solid-state perspective, a racemic mixture can crystallize in three ways: a racemic compound (hereafter called a 'racemate'), a racemic conglomerate (hereafter called a 'conglomerate') or a solid solution.[9] A racemate contains an equal ratio of both enantiomers in its crystal lattice with its molecules in a regular, usually centrosymmetric, arrangement.[10] A conglomerate is a physical mixture of both enantiomers that crystallize separately during the crystallization process; this is also referred to as spontaneous resolution.[11] A solid solution has both enantiomers present in the lattice in an unordered manner. It often happens when the two enantiomers compete for the same position in its crystal lattice, and the term "pseudo racemates" has also been used to describe this phenomenon.[12] Conglomerates are relatively rare, with this behavior observed for organic molecules about 5-10% cases in the Cambridge Structural Database, whereas racemates predominate and solid solutions occur rarely.[13-15] The importance of understanding the interaction between enantiomers of chiral compounds used as pharmaceuticals[16-17] has been highlighted through a recent report of a more stable racemic form of Pioglitazone Hydrochloride, which has been marketed as a conglomerate for many years.[18]

One of the common inexpensive methods to resolve the enantiomers of a compound on an industrial scale is the entrainment procedure, where the desired enantiomer is used as a seed in the crystallization step to obtain a pure product consisting only of the same enantiomer.[19-22] However, this method can only be used for chiral resolution when the compound crystallizes as a conglomerate.[23] Diastereomeric salt formation is a related method that has been used to crystallize the preferred enantiomer from a racemic mixture.[24]

Understanding the interconversion and stability relationships between racemic and conglomerate forms is an important step in the crystallization of an API.[25-31] In this context, we have examined the crystallization behavior of 3-methyl-2-phenylbutyramide, **1**, an antimitotic compound that

displays racemic and conglomerate forms, Figure 1. Notably, the solid-state properties of **1** have not been described previously.

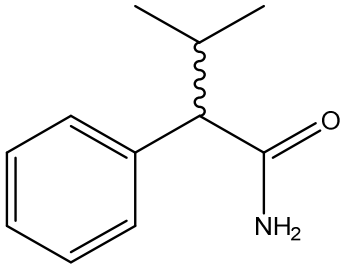

Figure 1. Structure of 3-methyl-2-phenylbutyramide, **1**.

Experimental

Materials and methods. Racemic 3-methyl-2-phenylbutyric acid was purchased from Alfa Aesar. (*R*)-3-Methyl-2-phenylbutyric acid was purchased from Sigma-Aldrich and (*S*)-3-methyl-2-phenylbutyric acid was purchased from Fluorochem. All solvents were purchased from Sigma-Aldrich and used directly, without any further purification.

(±)-3-Methyl-2-phenylbutyramide, (±)-1. This was synthesized from (±)-3-methyl-2-phenylbutyricic acid using the reported procedure.[32] ^{1}H NMR: δ_H (300 MHz, $CDCl_3$) : 7.38-7.23 (m, 5H), 5.47 (br s, 2H), 2.91 (d, J = 10.2 Hz, 1H), 2.48-2.30 (m, 1H), 1.08 (d, J = 6.5 Hz, 3H), 0.71 (d, J = 6.7 Hz, 3H). Anal. Calcd for $C_{11}H_{15}NO$: C, 74.54; H, 8.53; N, 7.90; Found: C, 74.29; H, 8.62; N, 7.98, mp: 105-107 ^{0}C. All spectroscopic details for **1** agreed with those previously reported.[32] Crystals suitable for single crystal analysis were grown from ethanol and called Form I.

(*R*)-3-Methyl-2-phenylbutyramide, (*R*)-1. To a flask containing (*R*)-3-methyl-2-phenylbutyric acid (0.15 g, 0.842 mmol) was added thionyl chloride (0.8 mL, 1.1 mmol, 1.3 equiv.) while maintaining the temperature at 0 °C. The solution was let warm to room temperature and stirred for 20 h. The excess thionyl chloride was removed under reduced pressure at room temperature to give a yellow liquid. This was dissolved in CH_2Cl_2 (1 mL) and the solution was added dropwise to aqueous ammonia solution (32%, 0.15 mL). This gave a white precipitate which was dissolved in CH_2Cl_2 (30 mL) and washed with water (3 x 20 mL) and brine (30 mL). The solvent was removed under *in vacuo* to give pure (*R*)-**1** as a white solid (0.140 g, 93%) with identical

spectroscopic characteristics to (±)-**1**. ^{1}H NMR: δ_H (300 MHz, $CDCl_3$): 7.38-7.23 (m, 5H), 5.47 (br s, 2H), 2.91 (d, J = 10.2 Hz, 1H), 2.48-2.30 (m, 1H), 1.08 (d, J = 6.5 Hz, 3H), 0.71 (d, J = 6.7 Hz, 3H), ^{13}C NMR δ (75 MHz, $CDCl_3$): 175.6, 139.1, 128.6, 128.3, 127.2, 61.1, 31.2, 21.6, 20.3. Anal. Calcd for $C_{11}H_{15}NO$: C, 74.54; H, 8.53; N, 7.90; Found: C, 74.64; H, 8.49; N, 7.83, m.p.: 138-140 °C.

(*S*)-3-Methyl-2-phenylbutyramide, (*S*)-1. This was synthesized from (*S*)-3-methyl-2-phenylbutyric acid following the procedure for (*R*)-**1** to give 0.143 g (95%) of pure (*S*)-**1**. ^{1}H NMR: δ_H (300 MHz, $CDCl_3$): 7.38-7.23 (m, 5H), 5.47 (br s, 2H), 2.91 (d, J = 10.2 Hz, 1H), 2.48-2.30 (m, 1H), 1.08 (d, J = 6.5 Hz, 3H), 0.71 (d, J = 6.7 Hz, 3H). Anal. Calcd for $C_{11}H_{15}NO$: C, 74.54; H, 8.53; N, 7.90; Found: C, 74.61; H, 8.48; N, 7.70, m.p.: 138-140 °C. Analysis matches the reported literature.[33]

Crystallization of conglomerate, Form I.

A wide variety of different crystallization conditions were examined. For all experiments Form I (~50 mg) was placed in a sample vial, solvent (10 mL) added and the sample vial heated gently until dissolution occurred. The resulting clear solution was filtered using a 0.45 micron filter fitted to a 10 mL syringe. A variety of different solvents and solvent mixtures were investigated: methanol, ethanol, acetonitrile, tetrahydrofuran, dichloromethane, water / methanol (50:50) and hexane / chloroform (50:50). For cooling crystallization experiments, the solutions were either allowed to cool to room temperature, or placed directly into the freezer compartment of a fridge (−4 °C). For solvent evaporation experiments, samples were left to stand at room temperature, or −4 °C, until dry. In certain instances, a rotary evaporator was used.[34,35]

Crystallization of (±)-Form II. The synthesized **(±)-1** (2.00 g, 11.3 mmol) was placed in the outer vessel of a sublimation apparatus, which was heated to 150 °C, and the internal cold finger was cooled with water circulating at ~10 °C. (At these conditions, **(±)-1** was in its liquid phase and vapors of **(±)-1** crystallized on the cold finger surface. No decomposition of **(±)-1** was observed) The outer vessel was maintained at 150 °C for 3 h, producing needle crystals of pure racemic Form II on the cold finger (1.86 g, 93% yield). Anal. Calcd for Form II crystals $C_{11}H_{15}NO$: C, 74.54; H, 8.53; N, 7.90; Found: C, 74.50; H, 8.55; N, 8.10, m.p.: 110-112 °C.

Crystallization of (±)-Form III. Crystals of Form II (1.00 g, 5.64 mmol) were placed in a 25 mL conical flask which was placed on a hot plate (~120 ºC) until all the solid had melted. Acetonitrile (10 mL) was added dropwise over 15 min. [Alternatively, the first step, heating until the solid melted, can be replaced by simply dissolving Form II in acetonitrile (10 mL)]. The resulting clear solution was removed from the hot plate, filtered using a 0.2 micron filter fitted to a 10 mL syringe, cooled to room temperature and placed into a fridge (−4 °C) for 2 d. Crystals of racemic Form III (blocks) and the conglomerate Form I (needles) crystallized concomitantly and were manually separated. Anal. Calcd for Form III crystals, $C_{11}H_{15}NO$: C, 74.54; H, 8.53; N, 7.90; Found: C, 74.58; H, 8.60; N, 8.12, m.p.: 112-114 °C.

Mechanical grinding. Mechanical grinding was carried out in a Retsch MM−00 Mixer mill, equipped with two stainless steel 5 mL grinding jars and one 2.5 mm stainless steel grinding ball per jar. The mill was operated at a rate of 30 Hz for 30 min and the typical sample size was 150-200 mg.

Slurry experiments. Slurry experiments were carried out with typically 150-200 mg of the sample placed in a 25 mL round bottomed flask, to which was added 2-3 mL of a solvent. After stirring for ~10 min at room temperature, 2-4 mg of seed crystals were added and the mixture stirred for a further 24 hours at room temperature. A detailed list of solvent, type of seed and the experimental outcomes are presented in Table 3 in the Supporting Information.

Manual grinding. Manual grinding was undertaken using a mortar and pestle with the typical sample size of 200-250 mg for 20 min. for both dry grinding and solvent drop grinding (using 2-3 drops of solvent).

Infrared Spectroscopy. Infrared spectra were recorded on a Bruker Tensor 37 attenuated total reflection (ATR)-IR spectrophotometer interfaced with Opus software version 7.2.139.1294 over a range of 400 – 4000 cm^{-1}. An average of 16 scans was taken for each spectrum obtained.

Powder X-Ray Diffraction. PXRD data were collected using a D2 phaser diffractometer using Cu Kα (λ = 1.5406 Å) radiation. Samples were analyzed over a 2θ range of 3.5−45° with increments of 0.05° at a rate of 2° min^{-1}. Data were evaluated using the DIFFRAC.Eva (Bruker AXS Inc.) software.

Nuclear Magnetic Resonance. ^{1}H (300 MHz) and ^{13}C (75.5 MHz) NMR spectra were recorded on a Bruker Avance 300 MHz NMR spectrometer. All spectra were recorded at room temperature (20 ºC) in deuterated chloroform ($CDCl_3$), using tetramethylsilane (TMS) as an internal standard. Chemical shifts (δ_H & δ_C) are reported in parts per million (ppm) relative to TMS and coupling constants are expressed in Hertz (Hz).

High Performance Liquid Chromatography (HPLC). Chiral HPLC analysis was conducted on a Waters Alliance 2690 separations module with a PDA detector. The enantiomeric purities were determined by analysis on a Chiralcel OD-H column (5 x 250 mm), purchased from Daicel Chemical Industries, Japan. The mobile phase was a 90:10 mixture of hexane:2-propanol, the flow rate was 1 mL min^{-1} and the detection wavelength was at 209.8 nm. The experiments were carried out at 25 °C.

Differential Scanning Calorimetry (DSC). All melting points were obtained from a TA Q1000 instrument. Samples (2–6 mg) were crimped in nonhermetic aluminum pans and scanned from 30 to 160 °C at a heating rate of 10 °C min^{-1} under a continuously purged dry nitrogen atmosphere.

Elemental analysis. An Exeter Analytical CE440 was used for elemental analysis.

Single Crystal X-ray Diffraction. Single crystal X-ray data was collected on a Bruker APEX II DUO diffractometer,[36] using graphite monochromatized Mo Kα (λ = 0.7107 Å) radiation for the racemic forms and Incoatec montel multilayer mirror monochromatized Cu Kα (λ = 1.5418 Å) radiation for the *R* and *S* enantiomers. The APEX suite of programmes,[37] incorporating the SHELX suite of programs,[38] were used. The structures were solved using direct methods and refined by full-matrix least-squares on F^2. All non-hydrogen atoms were located and refined with anisotropic thermal parameters. Hydrogen atoms were either placed in calculated positions or located and refined with isotropic thermal parameters. Diagrams were prepared with Mercury 3.8.[39] The crystallographic data are summarized in Table 1.

Table 1. Crystallographic data for both enantiomers and the two racemic forms

Compound	*R* Form	*S* Form	Form II	Form III

Formula	$C_{11}H_{15}N_1O_1$	$C_{11}H_{15}N_1O_1$	$C_{11}H_{15}N_1O_1$	$C_{11}H_{15}N_1O_1$
MW	177.24	177.24	177.24	177.24
crystal system	monoclinic	monoclinic	monoclinic	monoclinic
space group, *Z*	$P2_1$, 4	$P2_1$, 4	$P2_1/c$, 4	$P2_1/n$, 8
a, Å	15.0554(16)	15.0331(4)	12.017(6)	9.1071(10)
b, Å	5.2629(2)	5.26050(10)	5.158(3)	24.498(3)
c, Å	15.1388(6)	15.1573(4)	17.526(9)	10.49(2)
β, °	116.996(2)	116.9520(10)	93.757(13)	112.545(2)
V, Å^3	1068.82(7)	1068.47(5)	1084.0(10)	2141.2(4)
Dc, g cm^{-3}	1.101	1.102	1.086	1.100
Wavelength, Å	1.5418	1.5418	0.7107	0.7107
μ, mm^{-1}	0.552	0.552	0.069	0.069
θ range, deg	3.28-67.12	3.27-66.49	1.70-25.09	1.66-26.40
T, K	296	296	296	296
total reflns	10337	10451	12380	33023
unique reflns	3655	3643	1896	4390
R_{int}	0.0353	0.0205	0.0423	0.0287
obs. refns, $I > 2\sigma(I)$	3530	3570	1226	3647
no. parameters	255	255	152	255
no. restraints	1	1	0	0
R_1 [$I > 2\sigma(I)$]	0.0862	0.0320	0.0431	0.0448

wR_2 [all data]	0.2252	0.0877	0.1254	0.1175
S	1.135	1.052	1.010	1.082
Flack parameter	0.06(12)	0.08(6)	--	--
ρ_{max}, ρ_{min}, e Å^{-3}	0.893, -0.250	0.158, -0.129	0.221, -0.159	0.179, -0.169

Density Functional Theory Modelling

Density functional theory (DFT) simulations were applied to analyze the relative stability of the the different crystal forms of **1** and understand their energetic ordering. The initial crystal and atomic structures were taken from the experimental *.cif. DFT simulations were carried out using the VASP5.3[40] simulation code – the valence electrons were described in a periodic plane wave basis set with a cut off energy of 450 eV. The interaction between the core and valence electrons were described by the projector augmented wave approach[41] with 6, 5, 4 and 1 valence electron for O, N, C and H, respectively. The Perdew-Burke-Ernzerhof (PBE) GGA approximation to the exchange-correlation functional was applied.[42] Two hybrid DFT functionals were also applied, namely HSE06 and PBE0.[43,44] The HSE06 and PBE0 calculations use the default parameters of 25% exact HF exchange and, in HSE06, a screening length of 5 Å. Grimme's D2 and D3 models were used to include two different descriptions of the vdW interactions,[45,46] giving PBE-D2/PBE-D3, HSE06-D2/HSE06-D3 and PBE0-D2/PBE0-D3 theoretical models.

Initially, all atomic positions were relaxed with no symmetry imposed with convergence criteria in the energy and ionic relaxations of $1x10^{-5}$ eV and 0.01 eV Å^{-1}, respectively. Then the lattices were relaxed, with both lattice dimensions and angles being allowed to vary. We used direct lattice relaxations and an iterative procedure in which atomic positions are relaxed, followed by cell relaxation and repeating this process. The latter procedure avoids any issues arising from an incomplete plane wave basis set during simultaneous ion and cell relaxations; however, similar results were obtained for the lattice parameters in both approaches. Methfessel-Paxton Fermi level smearing was applied with a value of σ = 0.1 eV. The quasi-Newton relaxation algorithm was applied for the atomic relaxations.

Results and discussion

Conglomerate, Form I

(±)-3-Methyl-2-phenylbutyramide **1** was synthesized from (±)-3-methyl-2-phenylbutyric acid and crystallized from a variety of solvents. Crystals of Form I suitable for single crystal diffraction were obtained as needles by slow evaporation from ethanol and analysis revealed the *S* enantiomer had crystallized in the Sohncke space group $P2_1$ with $Z' = 2$. The experimental PXRD pattern of the synthesized amide matches the theoretical PXRD pattern based on this single crystal analysis, suggesting spontaneous resolution during crystallization and the formation of a conglomerate.

Analysis of 6 randomly picked crystals of Form I obtained from the ethanol crystallization batch revealed that they had all spontaneously resolved into the conglomerate, with no evidence of any other crystal form. This approach allowed both *R* and *S* enantiomers to be successfully characterized (both in $P2_1$ with $Z' = 2$). Difficulties were experienced in finding good quality single crystals, particularly for the *R* enantiomer, because most of the crystals stick to each other along the needle axis. By applying pressure with a needle, it was possible to separate the crystal, albeit with much smaller crystallites remaining adhered to the main needle. However, the absolute configurations of both enantiomers, (*R)*-**1** & (*S)*-**1**, have been established basing on the anomalous dispersion effects.

Crystal structure analysis of each enantiomer shows two crystallographically unique molecules in the asymmetric unit which interact with each other through infinite N-H···O=C hydrogen bonding. One of the amide hydrogen atoms forms $R_2^2(8)$ dimers, while the other amide hydrogen atom forms C(4) chains of the same symmetry molecules, also via N-H···O=C hydrogen bonding, leading to the well-known 1-D infinite ribbons, Figure 2.

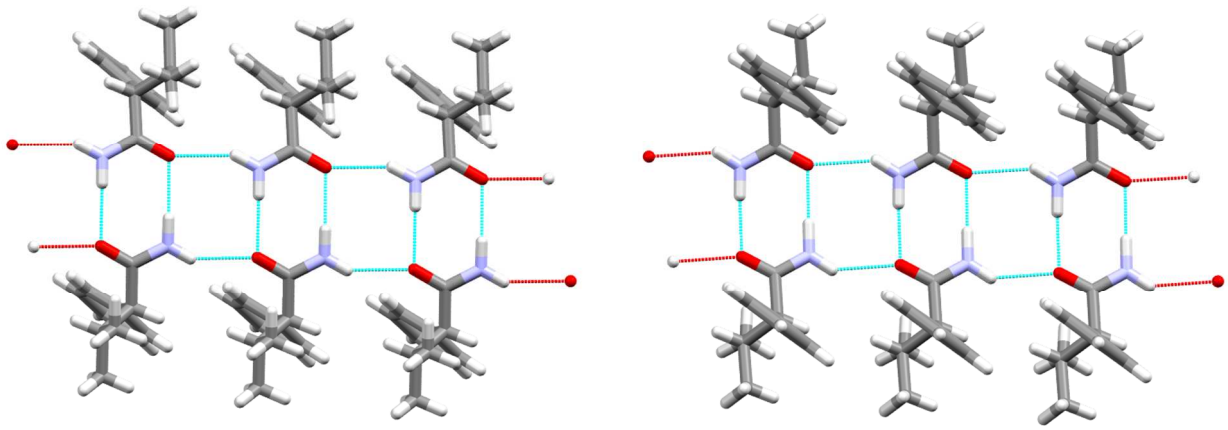

Figure 2. Crystal packing in *S* enantiomer (left) and *R* enantiomer (right).

To investigate further the formation of the conglomerate, the synthesis of the individual enantiopure enantiomers (*R*)-**1** and (*S*)-**1** was undertaken. While crystallization of either the *R* or *S* enantiopure material was attempted using a variety of solvents and crystallization techniques, crystals suitable for single crystal analysis could not be obtained in either case. However, the experimental PXRD pattern for samples of each enantiomer from these crystallization experiments match the calculated diffraction patterns generated from the single crystal data of Form I. The chiral HPLC analysis also confirms the spontaneous resolution during crystallization of (±)-**1** to form the conglomerate, Form I (see Supporting Information).

Racemic Polymorphs, Forms II and III

Crystallization of the amide was examined using a variety of methods including: fast and slow solvent evaporation in different organic solvents at different temperatures, crystallization from the melt by cooling to RT, mechanical grinding using either a mortar-pestle or a mixer mill, fast evaporation using a rotatory evaporator and melting followed by vapor crystallization.[47-49] Further details are provided in Table 3 in the Supporting Information. All these approaches yielded the conglomerate, except for evaporation from the melt, which gave rise to needle crystals of a new form that single crystal analysis revealed adopted the racemic space group $P2_1/c$ with $Z' = 1$, termed Form II. Subsequently, a third form, Form III, was obtained as block crystals concomitantly with Form I by crystallizing from acetonitrile and placing in a fridge at −4

°C (see Experimental). This was determined to be a second racemic form, crystallizing in $P2_1/n$ with $Z' = 2$. Different Z' values[50] are seen in Forms II and III.

In both Forms II and III, the amides interact *via* N-H···O=C hydrogen bonding by the formation of $R_2^2(8)$ dimers and C(4) chains to form the familiar ladder motif. For Form II, all the *R* enantiomers are located on one side of the ladder motif and the *S* enantiomers located on the opposite side due to inversion centers present in the middle of both the $R_2^2(8)$ dimers and the binary level $R_4^2(8)$ tetramers (Figure 3, left). In Form III, the inversion centers are only present in the middle of the $R_2^2(8)$ dimer, leading to an alternating arrangement of *R* and *S* enantiomers along each side of the ladder motif (Figure 3, right). The infinite ribbons are packed further in a parquet pattern in both forms.

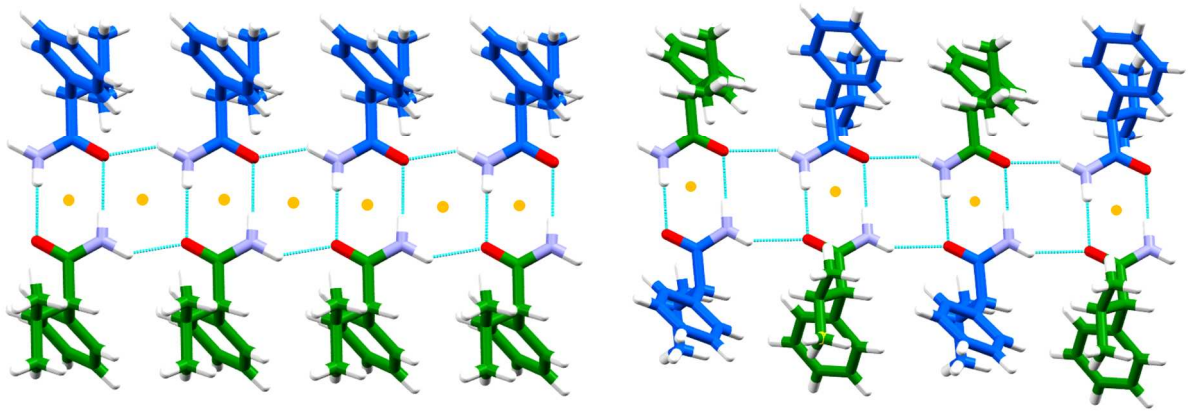

Figure 3 Comparison between the two racemic forms: Form II, left, and Form III, right. [*R* and *S* enantiomers, are colored blue and green, respectively, and the orange dots indicate the inversion centres.]

There are small, but significant, differences in the hydrogen bonding and IR data for the different forms, Table 2 (The IR data for the *R* and *S* Form are identical, so only the *S* Form is presented). The IR data for Form II for the C=O stretch (1699 cm^{-1}) and the N-H stretch (3161 cm^{-1}) are notably different to the corresponding data for Forms I, (1650 cm^{-1}, 3187 cm^{-1}) and III (1651 cm^{-1}, 3184 cm^{-1}). While this observation is not readily rationalized by analysis of bond lengths, angles, torsion angles and planarity of the nitrogen in the different forms, superimposition of the molecules indicate the conformation of the amides differ slightly across the three forms, presumably impacting on the IR data (see Figure 12 in the Supporting Information).

Table 2. Comparison of the different forms of **1**

	S Form	Form II	Form III
N-H···O=C, Å	2.08(2)	2.07(2)	1.985(2)
N-H···O, °	150.50(2)	142.97(2)	152.55(2)
$\nu_{C=O}$, cm^{-1}	1650	1699	1651
ν_{N-H}, cm^{-1}	3403, 3186	3393, 3161	3399, 3184
C=O Bond length, Å	1.228(2)	1.242(2)	1.234(2)
C-N Bond length, Å	1.326(3)	1.324(2)	1.325(2)

Interconversion experiments between conglomerate and racemates

In general, racemic compounds are thermodynamically more stable in comparison with the conglomerates.[51] Sublimation of racemic material can result in the formation of conglomerates.[52-55] It is rare for a conglomerate to convert to the racemate upon sublimation and we found only one report with such behavior.[56] Notably, in this reported case the conversion is a solid-to-solid process while in our work the racemate is formed by evaporation, i.e. melting followed by crystallization. Repeated experiments were undertaken to obtain sufficient quantities of the racemic Forms II and III. Both racemic forms readily reconvert to the conglomerate upon melting or recrystallization from solvents, suggesting that the conglomerate is more stable than either racemic form (see Table 3 in SI for details). As described earlier, Form II can be converted to a mixture of Forms I and III through low temperature crystallization from acetonitrile. Differential scanning calorimetry (DSC) revealed sharp melting endotherms and no high temperature transitions were seen for any of the forms. It has been reported that if the melting point of an enantiopure material is higher than that of the corresponding racemic material by 25 °C or greater, then that compound is expected to show spontaneous resolution behavior.[57] For **1** the differences in melting point between the *R* (or *S*) Form and Forms II and III are 28 °C and 26 °C, respectively, Table 3; spontaneous resolution is observed, in agreement with this empirical rule. A range of slurry experiments in different solvent media, both with and without seeding,

were performed to investigate the relative stability of the different forms. Form I was obtained exclusively in all the experiments, indicating that it is the most stable form in the conditions examined.

Table 3. Melting point for solid forms of **1**

Type of solid form	Melting point, °C
Form I [a]	105-108
***R* enantiomer**	138-140
***S* enantiomer**	138-140
Form II	110-112
Form III	112-114

[a] conglomerate of R and S

Mechanical grinding, an environmentally friendly method,[58,59] has been used to study the interconversion between polymorphs and establish their relative stabilities, although it does not necessarily yield the thermodynamically stable form.[60] Both manual (mortar-pestle) and mechanical (ball mill) methods were utilized for investigating the stability of the conglomerate and racemic forms of **1**. In all cases the conglomerate was the product obtained from the grinding experiments. Slurry crystallization and crystallization by seeding experiments also resulted in the transformation of the racemic forms to the conglomerate. The relationships between all the forms and routes to obtain them are summarized in Figure 4.

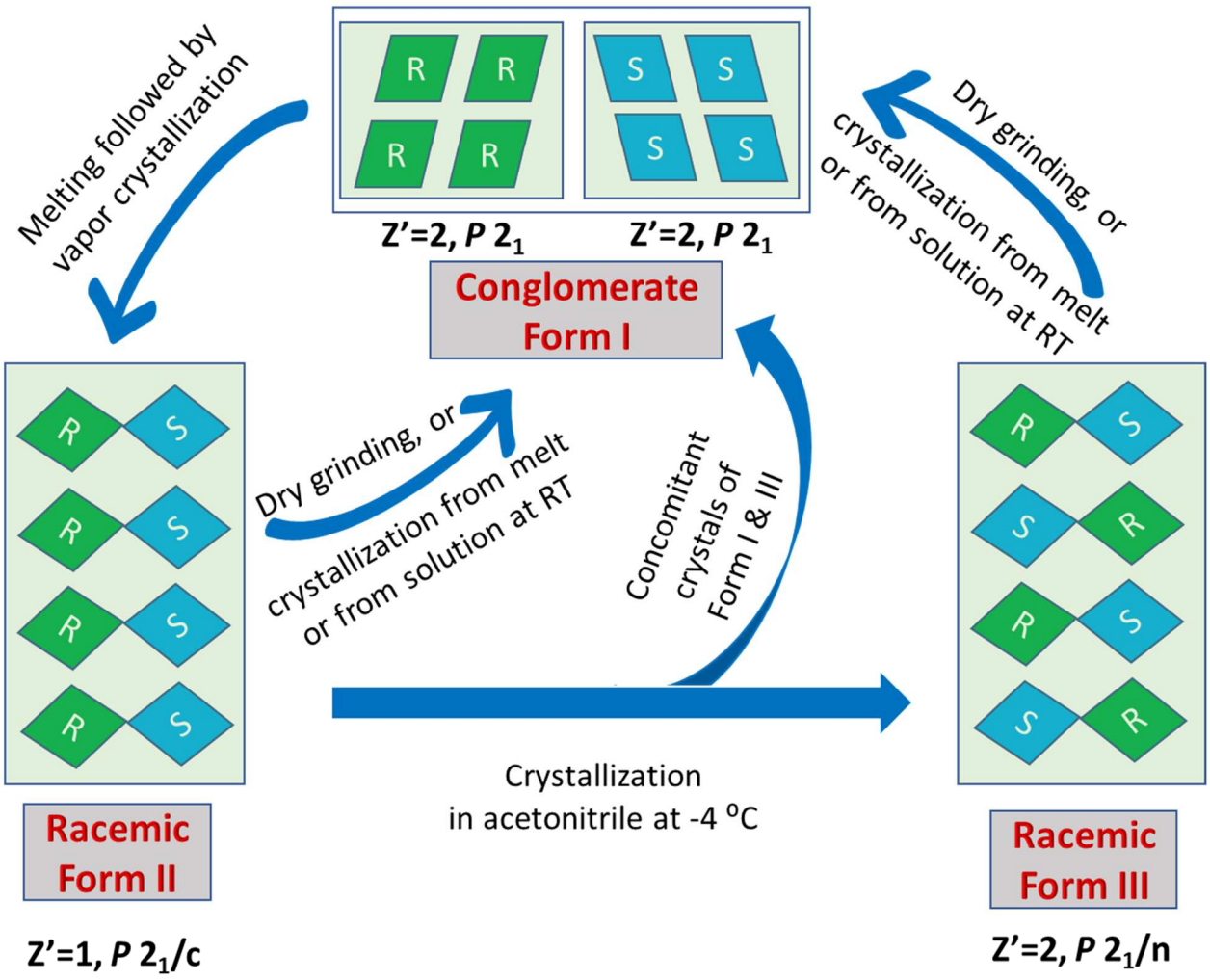

Figure 4. Schematic representation of the behavior of the solid forms of **1**.

DFT results on the stability of the crystal structures.

We have used density functional theory (DFT) simulations to examine the stability and structure of the crystal forms of **1** produced in the experiments. The DFT derived atomic structure of the *S* enantiomer, the *R* enantiomer and the two racemic forms, racemic Form-II and racemic Form-III that are derived from atomic and lattice relaxations are available in the SI. **Table 4** gives the computed lattice vectors and angles from the following DFT set-ups: PBE+vdW, HSE06+vdW and PBE0+vdW cell relaxations. The vdW interactions are the D2 and D3 and these are used for each exchange-correlation functional.

Comparison of the lattice parameters with the experimental data in Table 1 reveals that the PBE functional gives the smallest deviations from the experimental lattice parameters. By contrast, the HSE exchange-correlation functional can give very large deviations of up to 10% while the PBE0 functional can give deviations of *ca.* 5%, which is still significant. The crystal form that is most sensitive to the DFT set-up is the *R* form which shows the very strong deviations just described. This finding is robust to the choice of input structure, e.g. whether the relaxation begins from the experimental lattice or the PBE-D2 lattice. The cell angle β is much less senstive to the choice of DFT functional for each crystal form. Finally, the effect of the form of the vdW correction on the compuated lattice vectors and angles is much smaller and so the performance of both vdW corrections appears to be similar and, thus, it is the underlying exchange-correlation functional that gives the most significant differences.

Table 4. Computed lattice vectors and cell angle β for the enantiomers and racemic forms of **1.** The theoretical methods are explained as follows: **PBE-D2**: atomic and cell relaxations using PBE with Grimme D2 van der Waals correction. **PBE-D3**: atomic and cell relaxations using PBE with Grimme D3 van der Waals correction. **HSE06-D2**: atomic and cell relaxations using HSE06 with Grimme D2 van der Waals correction. **HSE06-D3**: atomic and cell relaxations using HSE06 with Grimme D3 van der Waals correction. **PBE0-D2**: atomic and cell relaxations using PBE0 with Grimme D2 van der Waals correction. **PBE0-D3**: atomic and cell relaxations using PBE0 with Grimme D3 van der Waals correction

PBE-D2				
	***S* Form**	***R* Form**	**Racemic Form II**	**Racemic Form III**
a, Å	14.603	14.556	11.398	8.932
b, Å	4.623	4.619	4.593	24.266
c, Å	14.691	14.598	17.453	10.016
β, °	117.33	117.4	92.970	112.041
PBE-D3				
	***S* Form**	***R* Form**	**Racemic Form II**	**Racemic Form III**
a, Å	14.696	14.629	11.740	8.937

b, Å	4.649	4.656	4.604	24.219
c, Å	14.791	14.675	17.616	10.034
β, °	117.359	117.237	93.021	112.08
HSE06-D2				
	***S* Form**	***R* Form**	**Racemic Form II**	**Racemic Form III**
a, Å	14.143	13.64	11.122	8.861
b, Å	4.547	4.446	4.526	24.135
c, Å	14.217	13.681	17.309	9.943
β, °	116.623	117.823	92.761	112.028
HSE06-D3				
	***S* Form**	***R* Form**	**Racemic Form II**	**Racemic Form III**
a, Å	14.168	12.778	10.968	8.854
b, Å	4.575	4.975	4.547	24.150
c, Å	14.242	12.8365	17.236	9.946
β, °	116.294	109.826	92.954	112.024
PBE0-D2				
	***S* Form**	***R* Form**	**Racemic Form II**	**Racemic Form III**
a, Å	14.304	13.071	11.216	8.881
b, Å	4.963	4.693	4.489	24.118
c, Å	14.405	13.111	17.362	9.962
β, °	116.041	114.925	92.706	112.061
PBE0-D3				
	***S* Form**	***R* Form**	**Racemic Form II**	**Racemic Form III**
a, Å	14.553	13.6004	11.223	8.906
b, Å	4.787	4.508	4.5001	24.209

c, Å	92.525	13.638	17.381	9.965
β, °	117.013	117.403	92.672	112.018

Table 5 provides the relative energies of each crystal form in kJ mol^{-1}, where the structure with zero energy is the most stable form. Together with the crystal structure data, this allows us to explore the suitabilitiy of, and any dependencies on, the choice of DFT exchange-correlation functional. From the energy data in **Table 5**, it appears that the *S* enantiomer and the *R* enantiomer are generally very close in energy, with a maximum difference of less than 1 kJ mol^{-1} with PBE-D2 or PBE-D3. This suggests that both enantiomers are equally likely to be formed. Considering the racemic forms, with PBE and both vdW correactions, these are both less stable and racemic Form III is by far the least stable.

However, with the hybrid DFT exchange-correlation functionals, there is a very strong effect on the relative energetics of the crystal forms, similar to the crystal structure. For example, with HSE06, the *R* enantiomer is now less stable than the racemic Form II, with the *S* enantiomer continuing to be the most stable. This is found with both vdW corrections so it appears to be attributable to the hybrid functional. With the PBE0+vdW hybrid functional, the qualitative trend in stability is the same as PBE+vdW, although we note that the relative energies from PBE0+vdW indicate that the racemic Form II is close in stabilty to the *R* enantiomer. Thus, it appears that there is a significant sensitivity in the crystal structure and, thus, stability to the DFT set-up and the standard hybrid DFT functionals appear to perform less well than the PBE GGA functional, irrespective of the vdW corrections used. This may be due to the contribution of exact exchange (25%) in PBE0 and HSE06 and, in addition, HSE06 has a screening length of 5 Å, which can influence the computational results. However, given the high cost of hybrid DFT calculations within the VASP code (*ca.* 50 times that of a GGA functional calculation), it is not practical to test hybrid DFT to obtain a an exact exchange contribution for each system . However, the PBE-GGA functional together with vdW corrections does appear to provide a reasonable description of the structure and stability of the MPBA system.

Table 5. Relative DFT energies in kJ mol^{-1} for the crystal forms of **1** studied. The energy of the most stable crystal form for a given DFT approach is set to 0 kJ mol^{-1}. The theoretical methods

are explained as follows: **PBE-D2**: atomic and cell relaxations using PBE with Grimme D2 van der Waals correction. **PBE-D3**: atomic and cell relaxations using PBE with Grimme D3 van der Waals correction. **HSE06-D2**: atomic and cell relaxations using HSE06 with Grimme D2 van der Waals correction. **HSE06-D3**: atomic and cell relaxations using HSE06 with Grimme D3 van der Waals correction. **PBE0-D2**: atomic and cell relaxations using PBE with Grimme D2 van der Waals correction. **PBE0-D3**: atomic and cell relaxations using PBE with Grimme D3 van der Waals correction

Crystal Structure	PBE-D2 $E^{relative}$ / kJ mol^{-1}	PBE-D3 $E^{relative}$ / kJ mol^{-1}	HSE06-D2 $E^{relative}$ / kJ mol^{-1}	HSE06-D3 $E^{relative}$ / kJ mol^{-1}	PBE0-D2 $E^{relative}$ / kJ mol^{-1}	PBE0-D3 $E^{relative}$ / kJ mol^{-1}
Racemic Form II	17	28	28	30	86	27
Racemic Form III	137	114	234	210	229	117
R enantiomer	0.2	0	188	173	17	35
S enantiomer	0	0.96	0	0	0	0

To help understand the differences in stability of the crystal forms we have examined the atomic structure and focused on the interactions between molecules of **1** in each crystal form. As discussed earlier, each structure has two N-H···O=C hydrogen bonds. The computational data using the PBE-D2 level of theory gave similar O···H distances of 1.98 Å in Form III, 2.08 Å in Form II, 1.96/2.02 Å in the *R* enantiomer and 2.07/2.09 Å in the *S* enantiomer. Thus, this cannot be the origin of the different stabilities observed. When we examine the different orientations of **1** in each form we note that the *R*, *S*, and racemic form II structures have adjacent aromatic rings, with typical H···H distances of 3.15 – 3.6 Å (typical benzene dimer distances are around 2.5 – 3.5 Å). However, the racemic Form III is the only structure with no adjacent aromatic rings. It is possible that this structure is less stable than the other forms of **1** because the stabilisation induced by the aromatic ring interactions is missing.

Conclusion:

In the antimitotic amide **1**, the most stable form in the solid state is a conglomerate, Form I. Two metastable racemic polymorphs have been identified, Forms II and III, notably with Form II isolated by melting Form I followed by vapor crystallization. The DFT energy calculations which include vdW corrections support our hypothesis that the individual enantiomers are more energetically favorable than the racemic polymorphs Form II and III. However, it appears that hybrid DFT in the guise of the HSE06 and PBE0 functionals with standard exchange contributions can have difficulty in describing these systems and, thus, care must be taken in applying hybrid DFT. Slurrying experiments revealed that the most stable form was the conglomerate in all conditions examined, in agreement with both the initial experimental results that identified the different forms and the computational results. This example highlights the need to explore as fully as possible the crystal landscape of conglomerates for potential polymorphs and the stability behavior of any polymorphs identified.

Electronic Supplementary Information (ESI) available. Detailed IR, PXRD, DSC data, and additional figures. The crystallographic data have been deposited with the Cambridge Crystallographic Data Centre, CCDC deposition numbers 1562052-1562055. This material is available free of charge via the Internet at http://pubs.acs.org.

Acknowledgment:

This publication has emanated from research conducted with the financial support of Science Foundation Ireland under Grant Numbers 12/RC/2275, 05/PICA/B802/EC07, 14/US/E2915 as well as the UCC 2012 Strategic Research Fund.

References:

1. Jamali, F.; Singh, N. N.; Pasutto, F. M.; Russell, A. S.; Coutts, R. T. Pharmacokinetics of Ibuprofen Enantiomers in Humans Following Oral Administration of Tablets with Different Absorption Rates *Pharm. Res.* **1988**, *5*, 40-43.
2. Vargesson, N. Thalidomide-induced limb defects: resolving a 50-year-old puzzle. *Bioessays,* **2009**, *31*, 1327-1336.
3. Ribeiro, A. R.; Castro, P. M. L.; Tiritan, M. E. Chiral pharmaceuticals in the environment *Environ. Chem. Lett.* **2012**, *10*, 239-253.

4. Sheldon, R. A. *Chirotechnology: Industrial synthesis of optically active pure compounds*; Dekker M: New York, 1993.

5. Caner, H., Groner, E., Levy, L., and Agranat, I. Trends in the development of chiral drugs *Drug Discovery Today* **2004**, *9*, 105-110.

6. Hutt, A. J.; Tan, S. C. Drug chirality and its clinical significance. *Drugs* **1996**, *52*, 1-12.

7. Rekoske, J. E. Chiral separations *AIChE J.,* **2001**, *47*, 2-5.

8. Lorenz, H.; Seidel-Morgenstern, A. Processes To Separate Enantiomers *Angew. Chem., Int. Ed.*, **2014**, *53*, 1218-1250.

9. Srisanga, S.; ter Horst, J. H. Racemic compound, conglomerate, or solid solution: phase diagram screening of chiral compounds *Cryst. Growth Des*. **2010**, *10*, 1808– 1812.

10. Moss, G. Basic terminology of stereochemistry (IUPAC Recommendations 1996) *Pure Appl. Chem.* **1996**, *68*, 2193-2222.

11. Sogutoglu, L.-C.; Steendam, R. R. E.; Meekes, H.; Vlieg, E.; Rutjes, F. P. J. T. Viedma ripening: a reliable crystallisation method to reach single chirality *Chem. Soc. Rev.* **2015**, *44*, 6723-6732.

12. Oliveira, M. A.; Peterson, M. L.; Klein, D. Continuously Substituted Solid Solutions of Organic Co-Crystals *Cryst. Growth Des.* **2008**, *8*, 4487-4493.

13. Jacques, J.; Collet, A.; Wilen, S. H. Enantiomers, Racemates, and Resolutions, Krieger Publishing Company, Malabar, FL, **1994**.

14. Gonella, S.; Mahieux, J.; Sanselme, M.; Coquerel, G. Spotting a Conglomerate Is Just Halfway to Achieving a Preparative Resolution by Preferential Crystallization *Org. Process Res. Dev.* **2012**, *16*, 286-293.

15. Li, Z. J.; Zell, M. T.; Munson, E. J.; Grant, D. J. Characterization of racemic species of chiral drugs using thermal analysis, thermodynamic calculation, and structural studies *J. Pharm. Sci*. **1999**, *88*, 337-346.

16. Khandavilli, U. B. R.; Lusi, M.; Bhogala, B. R.; Maguire, A. R.; Stein, M.; Lawrence, S. E. Diversity in a simple co-crystal: racemic and kryptoracemic behaviour *Chem. Commun*., **2016**, *52*, 8309-8312.

17. Carvalho Jr, P. S.; Ellena, J.; Yufit, D. S.; Howard, J. A. K. Rare Case of Polymorphism in a Racemic Fluoxetine Nitrate Salt: Phase Behavior and Relative Stability *Cryst. Growth Des*. **2016**, *16*, 3875-3883.

18. Zhang, C.; Matzger, A. J. A Newly Discovered Racemic Compound of Pioglitazone Hydrochloride Is More Stable than the commercial conglomerate *Cryst. Growth Des*. **2017**, *17*, 414-417.

19. Collet, A.; Brienne, M.-J.; Jacques, J. Optical resolution by direct crystallization of enantiomer mixtures *Chem. Rev.* **1980**, *80*, 215-230.

20. Wallach, O. Zur Kenntniss der Terpene und der ätherischen Oele. *Liebigs Ann. Chem.*, **1895**, *286*, 90-143.

21. Breuer, M.; Ditrich, K.; Habicher, T.; Hauer, B.; Kesseler, M.; Stürmer, R.; Zelinski, T. Industrial Methods for the Production of Optically Active Intermediates, *Angew. Chem., Int. Ed*. **2004**, *43*, 788-824.

22. Pallavicini, M.; Bolchi, C.;Binda, M.; Ferrara, R.; Fumagalli, L.; Piccolo, O.; Valoti, E. Entrainment resolution of carnitinamide chloride *Tetrahedron: Asymmetry* **2008**, *19*,1637-1640.

23. Subramanian, G. *Chiral Separation Techniques*, WILEY-VCH, Weinheim, 2nd edn, **2003.**

24. Brock, P.; Schweizer, W. B.; Dunitz, J. D.; On the validity of Wallach's rule: on the density and stability of racemic crystals compared with their chiral counterparts *J. Am. Chem. Soc.*, **1991**, *113*, 9811-9820.

25. Lorenz, H.; Langermann, von, J.; Sadiq, G.; Seaton, C. C.; Davey, R. J.; Seidel-Morgenstern, A.The Phase Behavior and Crystallization of 2-Chloromandelic Acid: The Crystal Structure of the Pure Enantiomer and the Behavior of Its Metastable Conglomerate *Cryst. Growth Des*. **2011**, *11*, 1549-1556.

26. Davey, R. J.; Sadiq, G.; Back, K.; Wilkinson, L.; Seaton, C. C. The isolation of a metastable conglomerate using a combined computational and controlled crystallization approach *Chem. Commun.* **2012**, *48*, 1976-1978.

27. Brandel, C.; Amharar, Y.; Rollinger, J. M.; Griesser, U. J.; Cartigny, Y.; Petit, S.; Coquerel, G. Impact of Molecular Flexibility on Double Polymorphism, Solid Solutions and Chiral Discrimination during Crystallization of Diprophylline Enantiomers *Mol. Pharmaceutics* **2013**, *10*, 3850-3861.

28. Davey, R. J.; Sadiq, G.; Seaton, C. C.; Pritchard, R. G.; Coquerel, G.; Rougeot, C. Racemic compound *versus* conglomerate: concerning the crystal chemistry of the triazoylketone, 1-(4-chlorophenyl)-4,4-dimethyl-2-(1*H*-1,2,4-triazol-1-yl) pentan-3-one *CrystEngComm*, **2014**, *16*, 4377-4381.

29. Braga, D.; Grepioni, F.; Shemchuk, O. Organic–inorganic ionic co-crystals: a new class of multipurpose compounds *CrystEngComm*, **2018**, DOI: 10.1039/C8CE00304A

30. Rekis, T.; Bērziņš, A.; Orola, L.; Holczbauer, T.; Actiņš, A.; Seidel-Morgenstern, A.; Lorenz, H. Single enantiomer's urge to crystallize in centrosymmetric space groups: solid solutions of phenylpiracetam *Cryst. Growth Des.* **2017**, 17, 1411-1418.

31. Tumanova,N.; Tumanov,N.; Robeyns,K.; Fischer,F.; Fusaro,L.; Morelle F.; Ban,V.; Hautier,G.; Filinchuk,Y.; Wouters,J.; Leyssens,T.; Emmerling, F. Opening Pandora's Box: Chirality, Polymorphism, and Stoichiometric Diversity in Flurbiprofen/Proline Cocrystals *Cryst. Growth Des.*, **2018**, *18*, 954-961.

32. Cervinka, O.; Dudek, V.; Hub, L. Asymmetric reactions. XXXIV. Absolute configuration of (S)-(+)-α-tert-butylphenylacetic acid, *Czechoslov. Chem. Commun*., **1970**, *35*, 724-726.

33. Cervinka, O.; Hub, L. Utilization of the asymmetric transformation to determine the absolute configuration of acids bearing an asymmetric carbon atom at the ex-position in respect to the carbonyl group, *Czechoslov. Chem. Commun*., **1967**, *32*, 2295-2300.

34. Kudelko, A.; Zielinski, W. An efficient synthesis of new 2-aminomethyl-1,3,4-oxadiazoles from enantiomeric phenylglycine hydrazides *Tetrahedron* **2009**, *65*, 1200-1206.

35. van Eupen, J.; Westheim, R.; Deij, M. A.; Meekes, H. The solubility behaviour and thermodynamic relations of the three forms of Venlafaxine free base *Int. J. Pharm.* **2009**, *368*, 146-153.

36. Eccles, K. S.; Stokes, S. P.; Daly, C. A.; Barry, N. M.; McSweeney, S. P.; O'Neill, D. J.; Kelly, D. M.; Jennings, W. J.; Ní Dhubhghaill, O. M.; Moynihan, H. A.; Maguire, A. R.; Lawrence, S. E. Evaluation of the Bruker SMART X2S: crystallography for the nonspecialist? *J. Appl. Crystallogr.* **2011**, *44*, 213-215.

37. APEX2 v2009.3-0; Bruker AXS: Madison, WI, **2009**.

38. Sheldrick, G. M. A short history of SHELX. *Acta Crystallogr., Sect. A.* **2008,** *64*, 112-122.

39. Macrae, C. F.; Bruno, I. J.; Chisholm, J. A.; Edgington, P. R.; McCabe, P.; Pidcock, E.; Rodriguez-Monge, L.; Taylor, R.; Van de Streek, J.; Wood, P. A. Mercury CSD 2.0 - new features for the visualization and investigation of crystal structures *J. Appl. Crystallogr.* **2008**, *41*, 466-470.

40. Kresse, G.; Furthmüller, J., Efficiency of ab-initio total energy calculations for metals and semiconductors using a plane wave basis set, *Comp. Mat. Sci.*, **1996**, *6***,** 15-50.

41. Kresse, G.; Joubert, D., From ultra-soft pseudopotentials to the project wave augmented method, *Phys. Rev. B*, **1999**, *59***,** 1758-1775.

42. Perdew, J. P.; Burke, K.; Ernzerhof, M., Generalised gradient approximation made simple, *Phys, Rev. Lett.*, **1996**, *77***,** 3865-3869.

43. Perdew, J. P.; Ernzerhof, M.; Burke, K. Rationale for mixing exact exchange with density functional approximations. *J. Chem. Phys.*, **1996**, *105*, 9982–9985.

44. Adamo, C.; Barone, V. Toward reliable density functional methods without adjustable parameters: The PBE0 model. *J. Chem. Phys*., **1999**, *110*, 6158–6170.

45. Grimme, S.; Antony, J.; Ehrlich, S.; Krieg, H. A consistent and accurate ab initio parametrization of density functional dispersion correction (DFT-D) for the 94 elements H-Pu *J. Chem. Phys.* **2010**, *132*, 154104-*1*-154104-*19*.

46. Grimme, S. Semiempirical GGA-type density functional constructed with a long-range dispersion correction. *J. Comput. Chem.* **2006**, *27*, 1787–1799.

47. Zhang, G. G: Z.; Paspal, S. Y. L.; Suryanarayanan, R.; Grant, D. J. W. Racemic species of sodium ibuprofen: Characterization and polymorphic relationships *J. Pharm. Sci.* **2003**, *92*, 1356-1366.

48. Tarasevych, A. V.; Sorochinsky, A. E.; Kukhar, V. P.; Chollet, A.; Daniellou, R.; Guillemin, J.-C. Partial Sublimation of Enantioenriched Amino Acids at Low Temperature. Is it Coming From the Formation of a Euatmotic Composition1 of the Gaseous Phase? *J. Org. Chem.*, **2013**, *78*, 10530-10533.

49. Isakov, A. I.; Kotelnikova, E. N.; Kryuchkova, L. Y.; Lorenz, H.Effect of crystallization conditions on polymorphic diversity of malic acid RS — Racemate *Trans. Tianjin Univ.* **2013**, *19*, 86-91.

50. Steed, K. M.; Steed, J. W. Packing Problems: High Z′ Crystal Structures and Their Relationship to Cocrystals, Inclusion Compounds, and Polymorphism *Chem. Rev.* **2015**, *115*, 2895– 2933.

51. Li, J. Z.; Grant, D. J. W. Relationship Between Physical Properties and Crystal Structures of Chiral Drugs *J. Pharm. Sci.* **1997**, *86*, 1073-1078.

52. Perry, R. H.; Wu, C. P.; Nefliu, M.; Cooks, R. G. Serine sublimes with spontaneous chiral amplification, *Chem. Commun*. **2007**, *10*, 1071-1073.

53. Han, J.; Nelson, D. J.; Sorochinsky, A. E.; Soloshonok, V. A. Self-Disproportionation of Enantiomers via Sublimation; New and Truly Green Dimension in Optical Purification *Curr. Org. Synth.* **2011**, *8*, 310-317.

54. Viedma, C.; Noorduin, W. L.; Ortiz, J. E.; de Torres, T.; Cintas, P. Asymmetric amplification in amino acid sublimation involving racemic compound to conglomerate conversion, *Chem. Commun.* **2011,** *47*, 671-673.

55. Tarasevych, V.; Sorochinsky, A. E.; Kukhar, V. P.; Guillemin, J. -C. High temperature sublimation of α-amino acids: a realistic prebiotic process leading to large enantiomeric excess *Chem. Commun.* **2015**, *51*, 7054-7057.

56. Aceña, J. L.; Sorochinsky, A. E.; Katagiri, T.; Soloshonok, V. A. Unconventional preparation of racemic crystals of isopropyl 3,3,3-trifluoro-2-hydroxypropanoate and their unusual crystallographic structure: the ultimate preference for homochiral intermolecular interactions *Chem. Commun.* **2013**, *49*, 373-375.

57. Pérez-García, L.; Amabilino, D. B. Spontaneous resolution under supramolecular control *Chem. Soc. Rev.* **2002**, *31*, 342-356.

58. Friščić, T.; Halasz, I.; Beldon, P. J.; Belenguer, A. M.; Adams, F.; Kimber, S. A. J.; Honkimäki, V.; Dinnebier, R. E. Real-time and in situ monitoring of mechanochemical milling reactions *Nat. Chem*. **2013**, *5*, 66-73.

59. James, S. L.; Adams, C. J.; Bolm, C.; Braga, D.; Collier, P.; Friščić, T.; Grepioni, F.; Harris, K. D. M.; Hyett, G.; Jones, W.; Krebs, A.; Mack, J.; Maini, L.; Orpen, A. G.; Parkin, I. P.; Shearouse, W. Ch.; Steed, J. W.; Waddell, D. C. Mechanochemistry: opportunities for new and cleaner synthesis *Chem. Soc. Rev*. **2012**, *41*, 413-447.

60. Trask, A. V.; Shan, N.; Motherwell, W. D. S.; Jones, W.; Feng, S.; Tan, R. B. H.; Carpenter, K. J. Selective polymorph transformation via solvent-drop grinding *Chem. Commun*. **2005**, 880-882.

For Table of Contents Use Only

Exploring the crystal landscape of 3-methyl-2-phenylbutyramide: crystallization of metastable racemic forms from the stable conglomerate

U. B. Rao Khandavilli, Declan P. Gavin, Anita R. Maguire, Michael Nolan, Simon E. Lawrence

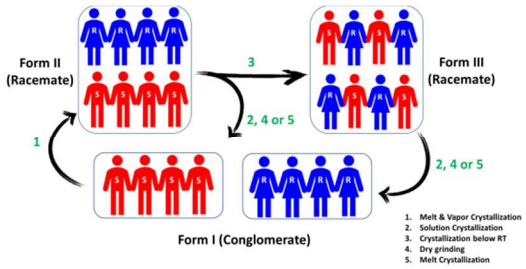

Three polymorphs have been identified for the antimitotic amide (±)-3-methyl-2-phenylbutyramide: a stable conglomerate and two metastable racemates, as evidenced by both experimental and theoretical studies. The more stable racemate is obtained by melting the conglomerate and crystallizing from the vapor, a rare phenomenon.